ADVANCING EARTH AND SPACE SCIENCES

Geophysical Research Letters

RESEARCH LETTER
10.1029/2026GL122310

Airborne Observations Reveal Underestimated Riverine Methane Emissions Across the Amazon

Linda Ort[1], Christian Frankenberg[2,3], Nikhil Dadheech[4], James (Young Suk) Yoon[4], Alexander J. Turner[4], A. Anthony Bloom[3], Paul Konopka[5], Hans-Christoph Lachnitt[6], Peter Hoor[6], Jos Lelieveld[1,7], Eric A. Kort[1,8], and Horst Fischer[1]

[1]Atmospheric Chemistry Department, Max Planck Institute for Chemistry, Mainz, Germany, [2]Division of Geological and Planetary Sciences, California Institute of Technology, Pasadena, CA, USA, [3]Jet Propulsion Laboratory, California Institute of Technology, Pasadena, CA, USA, [4]Department of Atmospheric and Climate Science, University of Washington, WA, WA, USA, [5]Institute of Climate and Energy Systems, Stratosphere (ICE-4), Forschungszentrum Jülich, Jülich, Germany, [6]Institute for Atmospheric Physics, Johannes Gutenberg University, Mainz, Germany, [7]Climate and Atmosphere Research Center, The Cyprus Institute, Nicosia, Cyprus, [8]Climate and Space Sciences and Engineering, University of Michigan, Ann Arbor, MI, USA

Key Points:

- Regionally enhanced methane mixing ratios have been observed over the Amazon Basin about twice those simulated by bottom-up models
- Wetland emissions are underestimated by a factor up to four in and near rivers
- Largest fractional methane flux underestimations are linked primarily to large river deltas, reservoirs, and flooded areas in the Amazon

Supporting Information:

Supporting Information may be found in the online version of this article.

Correspondence to:

L. Ort,
linda.ort@mpic.de

Citation:

Ort, L., Frankenberg, C., Dadheech, N., Yoon, J. (Y. S.), Turner, A. J., Bloom, A. A., et al. (2026). Airborne observations reveal underestimated riverine methane emissions across the Amazon. *Geophysical Research Letters*, *53*, e2026GL122310. https://doi.org/10.1029/2026GL122310

Received 19 FEB 2026
Accepted 22 JUN 2026

Author Contributions:

Conceptualization: Linda Ort, Christian Frankenberg, Horst Fischer
Data curation: Linda Ort, Nikhil Dadheech, James (Young Suk) Yoon, A. Anthony Bloom, Paul Konopka, Hans-Christoph Lachnitt
Formal analysis: Linda Ort
Funding acquisition: Jos Lelieveld, Horst Fischer
Investigation: Linda Ort
Methodology: Linda Ort, Alexander J. Turner
Project administration: Linda Ort, Christian Frankenberg, Horst Fischer
Resources: Linda Ort
Software: Linda Ort, Nikhil Dadheech
Supervision: Peter Hoor, Horst Fischer
Validation: Linda Ort
Visualization: Linda Ort

Abstract Strongly increasing trends in global methane in recent decades highlight the importance of understanding source-sink attributions and climate feedback mechanisms, especially for large natural sources like wetlands. Here, we present an analysis of airborne methane observations above the Amazon Basin conducted from December 2022 through January 2023 that reveal enhanced methane concentrations, especially below 6 km. Using Bayesian inversion with the atmospheric transport model STILT, we optimize surface fluxes to match our observations, starting from prior bottom-up flux estimates by WetCHARTs. The posterior suggests underestimated emissions across the Amazon Basin. The largest underestimates occur along rivers and tributaries, where emissions exceeded model values by up to a factor of four. River deltas make up 26% of the underestimated fluxes with reservoirs, and regularly flooded riverine areas contribute 19% and 13%, respectively. This highlights the need for improved understanding of the continuum across wetlands and freshwaters for tropical methane emissions.

Plain Language Summary Methane is a powerful greenhouse gas, and its rapid increase in the atmosphere over recent decades highlights the need to better understand its sources and how it influences the climate. In this study, we analyzed methane measurements taken from aircraft over the Amazon Basin between December 2022 and January 2023. The data showed high methane levels, especially in the lower atmosphere below 6 km. We found the methane emissions were previously underestimated by up to a factor of four. The underestimates were predominately along rivers and tributaries. Our work highlights the need for improved understanding of methane emissions from river systems in the tropics.

1. Introduction

Methane (CH_4), the second most important anthropogenic greenhouse gas after CO_2, has a global warming potential of approximately 25 over a 100-year time horizon, and its atmospheric concentration is projected to continue rising (Dhakal et al., 2022; Uluocak, 2025). The renewed growth of atmospheric methane since 2007 has coincided with isotopic lightening (declining $\delta^{13}C\text{-}CH_4$) (Lan et al., 2025; Nisbet et al., 2019), suggesting a shift toward stronger biogenic sources, such as from wetlands or cattle (Niwa et al., 2025; Turner et al., 2019).

Owing to its strong radiative forcing and relatively short atmospheric lifetime of roughly 9 years (Prather et al., 2012) compared to most other greenhouse gases, methane is a key target for near-term climate mitigation, as emission reductions can rapidly lower atmospheric concentrations and limit additional warming (Jackson et al., 2020; Pérez-Domínguez et al., 2021; Predybaylo et al., 2025; Shindell et al., 2012). Realizing this potential, however, requires a robust understanding of the spatiotemporal balance between methane sources and sinks.

Methane emissions arise from both anthropogenic (65% of total emissions, e.g., agriculture, fossil fuel exploitation, biomass burning, waste management) and natural sources (35%, e.g., wetlands, inland freshwater, permafrost, microbial activity). As international agreements (e.g., Paris Agreement, Global Methane Pledge, i.e., (Malley et al., 2023)) aim to regulate anthropogenic methane emissions, uncertainties in natural sources may

Writing – original draft: Linda Ort
Writing – review & editing: Christian Frankenberg, Nikhil Dadheech, James (Young Suk) Yoon, Alexander J. Turner, A. Anthony Bloom, Paul Konopka, Hans-Christoph Lachnitt, Peter Hoor, Jos Lelieveld, Eric A. Kort, Horst Fischer

become an even stronger limiting factor in constraining the global methane budget. In addition, wetland and freshwater environments are increasingly sensitive to human influences, such as climate change, land-use change, and eutrophication (Saunois et al., 2020, 2024, 2025; Zhang et al., 2017; Zhu et al., 2025).

Global methane emission estimates have improved substantially in recent years. This progress is reflected by the narrowing gap between top-down (575 Tg yr^{-1}) and bottom-up (669 Tg yr^{-1}) estimates for 2010–2019 (Saunois et al., 2025). This corresponds to a ∼16% overestimate in current bottom-up inventories, about half of the ∼30% discrepancy reported previously (Saunois et al., 2020). The improvement is largely attributed to an improved representation of natural emissions, which still exhibit the largest uncertainties (Zhu et al., 2025). Methane emissions are highly variable in space and time, and localized point sources can dominate regional budgets (Cusworth et al., 2022; Frankenberg et al., 2016; He et al., 2024; Jacob et al., 2022). While including additional sources from inland freshwaters (e.g., reservoirs, lakes, ponds, streams, and rivers) as well as refined process descriptions (e.g., hysteretic temperature sensitivity) (Chen et al., 2025; Delwiche et al., 2022; Saunois et al., 2024; Saunois et al., 2025) reduces double counting between freshwater and wetland emissions, and implies feedback mechanisms from anthropogenic activities (Saunois et al., 2025). However, methane observations from satellites, surface networks (FLUXNET-CH_4), or other in situ (e.g., airborne) data best improve emission estimates (Delwiche et al., 2021; Knox et al., 2019; Lu et al., 2021).

Tropical wetlands account for the largest share of global methane emissions, but limited ground stations and persistent deep cloud cover pose major challenges for ground and satellite observational data coverage, respectively (Asner, 2001). Airborne measurements, on the other hand, have advantages in tropical regions as they are able to collect high-resolution in situ data independent from the infrastructure and cloud cover. Airborne measurements can resolve boundary layer structure, the free troposphere, and entrainment zones vertically, spatially, and temporally (Andreae et al., 2012; Basso et al., 2021; Beck et al., 2012; France et al., 2022). Combined with transport models and inverse simulation methods (e.g., Bayesian inversion), airborne observations provide valuable insights on regional surface fluxes.

The Amazon rain forest is known to be a strong methane emitter due to its high wetland emissions (Pangala et al., 2017; Saunois et al., 2025; Zhu et al., 2025). Here, wetlands contribute to 83% of the forest's total methane emissions, followed by seasonal biomass burning emissions (17%) that occur largely during the region's dry fire season (Jul–Oct) (Basso et al., 2021; Saunois et al., 2020). Several previous airborne campaigns have identified large fluxes from wetlands in Bolivia or south-east Amazonia (Basso et al., 2021; France et al., 2022). However, the high complexity of wetland regions in parameters such as soil physical properties, vegetation type and water availability through flooding and precipitation, are not fully captured by the spatiotemporal resolution of current models (Dutaur & Verchot, 2007). Therefore, more observations are crucial to understand the Amazon methane budget and its changes over time due to human activity, such as large-scale deforestation (Silva Junior et al., 2021), floodings through hydropower stations (Caldas et al., 2023; Michael Keller, 1994), and a changing climate.

In this study, we use dense in situ observations of methane from a recent airborne campaign over the Amazon with observations ranging from the planetary boundary layer (PBL) to the upper troposphere, covering altitudes between 200 m up to 14.5 km. We use this spatially-dense set of observations to evaluate current wetland emission inventories. We also use a high resolution Lagrangian Particle Dispersion Model (LPDM) to relate these airborne observations to surface fluxes. Finally, we identify regions that are over- or underestimated in the process-based wetland model via Bayesian inference.

2. Observed Enhancements and Inversion Framework

In a previous study (Ort et al., 2024), we observed regional enhancements of dry methane mixing ratios over the Amazon Basin from December 2022 to January 2023 with research flights every 2–4 days. This airborne data, measured by the Airborne Tropospheric Tracer in situ Laser Absorption spectrometer (ATTILA) via infrared quantum cascade laser absorption spectroscopy (QLAS) (Ort et al., 2024), was conducted during the Chemistry of the Atmosphere Field Experiment in Brazil (CAFE Brazil) (Curtius et al., 2024; Nussbaumer et al., 2024). Depending on the measurement platform, uncertainty contributions can change (Röder et al., 2024). Therefore, we use frequent in-flight calibrations to derive a measurement uncertainty of $\sigma = \pm 67.69$ ppb for one-minute averaged data over the whole campaign. Higher uncertainties are expected during rapid ascents and descents.

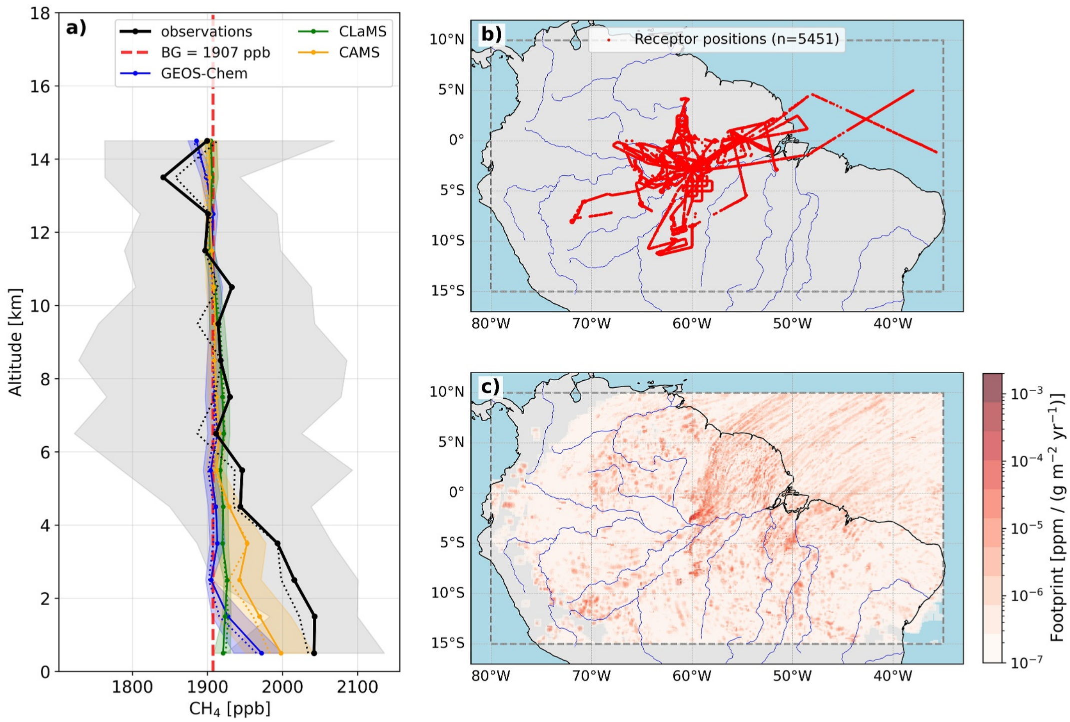

Figure 1. Methane observations and their footprints. Panel (a) shows the mismatch between observed methane vertical profiles (black lines) and three model simulations (CAMS: orange lines, GEOS-Chem: blue lines, CLaMS: green lines), each interpolated along the flight tracks. The vertical profiles are derived from the 60 s-data points, averaged over 1 km-boxes over the whole Amazon region, defined from 80°W–35°W and 15°S–10°N (gray grid box in (b, c)). Solid and dotted lines represent the means, and medians, respectively, and the shaded areas the 25th and 75th percentiles. The three modeled data sets were intentionally merged with the free tropospheric mean value of the observations (background; BG = 1907.46 ppb; red line) by applying a relative factor shifting the vertical profile to match the BG. Panel (b) shows the receptor positions (60 s data point aircraft position) that result in a valid footprint, superimposed in panel (c). The footprints are purely dynamical, meaning they represent any gas particle concentration per unit flux over the whole CAFE Brazil campaign. Units were converted to ppm $(g\ m^{-2}\ yr^{-1})^{-1}$ using the molar mass of methane for consistency.

Therefore, data taken during those periods were set to the maximum possible uncertainty of $\sigma = \pm 315.35$ ppb, which is derived from the in-flight calibrations before linear correction. See Section S1 in Supporting Information S1 for further details.

Figure 1 shows a comparison of the airborne observations from CAFE Brazil with three different models: CAMS (Copernicus Atmosphere Monitoring Service, Bergamaschi et al. (2013)), GEOS-Chem (Bey et al., 2001; Henze et al., 2007; Maasakkers et al., 2019), and CLaMS (Chemical Lagrangian Model of the Stratosphere, version 3.0, McKenna, Konopka, et al. (2002); McKenna, Grooß, et al. (2002); Konopka et al. (2025)). CAMS, GEOS-Chem, and CLaMS differ in their treatment of transport and emissions. Additional information on the models is provided in Text S2 of Supporting Information S1.

We find systematic enhancements in the airborne observations from the surface up to 6 km compared to all three models, with the largest enhancements below 4 km. Above ~6 km, all models and the aircraft observations show a uniform profile with comparable variability (background = 1,907 ppb). In the aircraft observations, we observed a mean enhancement of approximately 135 ppb at the lowest altitudes (below 1 km) relative to the free tropospheric background in both months of observations (Dec: 2042.98 ppb; Jan: 2041.13 ppb). We expected stronger variability at higher altitudes due to convective activity, which has also been observed through elevated carbon monoxide and isoprene mixing ratios in the free and upper troposphere (see Curtius et al., 2024; Ort et al., 2024). However, convection is often poorly represented in models (i.e., Prein et al. (2015)).

The upwind region of the measurements that influence the observed concentration, known as the measurement “footprint”, is calculated with the STILT model, a Lagrangian model built upon the Hybrid Single-Particle

Lagrangian Integrated Trajectory (HYSPLIT) model (Dadheech et al., 2025; Lin et al., 2003; Turner et al., 2018). STILT can generate time-resolved footprints (e.g., hourly) using meteorological data from the GFS (Global Forecast System) and particle dispersion from a starting location, known as receptor position. This produces a 3-D array (x, y, t) that can be integrated over time to yield a two-dimensional footprint matrix unique to each observation. This footprint matrix relates surface fluxes to the in situ airborne observations.

The spatial domain of our study ranges from 80°W–35°W and 15°S–10°N (marked as gray dashed box in Figures 1b and 1c) with a horizontal grid resolution of $0.1° \times 0.1°$. The resulting domain comprises approximately 10^5 grid cells (m = latitudes $\times$ longitudes = 249 $\times$ 449 = 111,801). Here, footprints were calculated for each 60 s-averaged observation as receptor positions shown in Figure 1b. In total, we have 7,620 receptor positions. Of these, the back trajectories for 2,169 receptors have no sensitivity to surface emissions within the defined spatial and time (five days backward) domain. As such, we use n = 5,451 receptors with non-zero surface sensitivity for this analysis. A superposition of all footprints is shown in Figure 1c. Approximately 89% of the domain is covered with at least one trajectory endpoint per cell; however, we focus on regions with the 40% highest sensitivity from the observations, quantified by the total number of trajectory-endpoints and total fraction of particles arriving in each cell (see Figure S4 in Supporting Information S1). The large number of observations combined for each grid cell within this region enhances statistical robustness and thereby reduces observational uncertainty. See Text S3 in Supporting Information S1 for details.

As mentioned above, we relate the observational enhancement toward the background concentration $\mathbf{y}$ $(n \times 1)$ to the surface emissions $\mathbf{x}$ $(m \times 1)$ using the footprint matrix: $\mathbf{y} = \mathbf{Hx}$, where $\mathbf{H}$ being the footprint matrix of shape $(n \times m)$. To infer the emissions $\mathbf{x}$ from the observed concentrations, we can minimize a cost function following Rodgers (1990, 2000). The resulting solution (posterior emissions; $\hat{\mathbf{x}}$) to this inverse problem can be estimated as follows:

$$\hat{\mathbf{x}} = \mathbf{x}_p + \mathbf{BH}^T\left(\mathbf{HBH}^T + \mathbf{R}\right)^{-1}(\mathbf{y} - \mathbf{Hx}_p). \tag{1}$$

Here, $\mathbf{x}_p$ is the prior emission inventory and is used to provide a baseline estimate of the emissions, weighted with its error covariance matrix $\mathbf{B}$. The observational uncertainty is provided with the observational covariance matrix $\mathbf{R}$. The inversion was solved in observation space by forming the system $\mathbf{HBH}^T + \mathbf{R}$ and solving the resulting linear equation directly, thereby avoiding explicit matrix inversion. The posterior estimate was obtained by weighting across the prior covariance and adjoint transport operator, yielding a solution equivalent to the classical Bayesian formulation (Rodgers, 2000; Tarantola, 2005) but computationally efficient for large state dimensions.

We use WetCHARTs (v1.3.3, spatial resolution: $0.5° \times 0.5°$, Bloom et al., 2024) bottom-up estimates as our prior emission inventory, as it has previously been shown to capture regional-scale spatial distribution of methane wetland emissions over South America (Benavente et al., 2026; Hancock et al., 2025; Zhu et al., 2025). WetCHARTs assumes comparatively strong emissions over the region of interest (Figure S15 in Supporting Information S1) and was therefore selected as the prior expected to provide the closest agreement with the observations. Anthropogenic emissions within the domain are considered negligible based on available emission inventories (see Figures S13 and S14 in Supporting Information S1) and literature (Curtius et al., 2025). For the prior state vector $\mathbf{x}_p$ we use the ensemble mean of December and January WetCHARTs simulations (2001–2022) that were generated, from different wetland extents, terrestrial biosphere models, and CH_4 : C temperature dependencies. Therefore, WetCHARTs includes emissions from wetlands and inland freshwaters, naturally or artificially created.

Additional consideration was given to the construction of the prior error covariance matrix ($\mathbf{B}$, $m \times m$) and the observational covariance matrix ($\mathbf{R}$, $n \times n$). For the prior error covariance matrix, fine-grid ensemble variances are scaled first such that the aggregated covariance within each coarse grid cell reproduces the original WetCHARTs ensemble uncertainty. Afterward, we follow Turner et al. (2020) by constructing the prior covariance with spatial correlations based on land-cover similarity. Here, we use Global Lakes and Wetlands Database (GLWD, version 2, Lehner et al., 2025a) and exponentially decay correlations in distance, such that approximately one-and-a-half coarse grid cells are covered. This spatial correlation ensures that when the

10.1029/2026GL122310

inversion increases emissions in a given grid cell, neighboring cells of the same land-cover type within a defined radius also adjust their emissions, with the magnitude of the adjustment decreasing with distance (see Section S4.1 and Figure S6 in Supporting Information S1 for more detail). For **R**, we take the variance over all in-flight calibrations $\left(\mathrm{diag}(\mathbf{R}) = \sigma^2\right)$ while assuming no correlation between each observation, resulting in a diagonal covariance matrix ($n \times 1$) for the inversion.

For large systems, it is computationally infeasible to store the posterior flux uncertainty **P** explicitly. Therefore, the random probe Hutchinson estimator was used to approximate its diagonal elements, providing grid-level posterior standard deviations $\left(\hat{\sigma}_{i,i} \approx \sqrt{\mathbf{P}_{i,i}}\right)$. This stochastic trace estimation method efficiently samples random perturbations to estimate the variance reduction in each grid cell (Hutchinson, 1989; Scheuer & Stoller, 1962). Furthermore, we calculate the averaging kernel sensitivity, which is a dimensionless measure of information gain that indicates the fraction of the posterior flux signal driven by the observations, as the diagonal elements of the posterior averaging kernel mapped onto the coarse flux grid. More details on the inversion settings are available in Text S4 in Supporting Information S1.

3. High Resolution Methane Fluxes

The resulting posterior emissions using airborne observations and WetCHARTs bottom-up estimates are shown in Figure 2. The left panels present the results for the entire domain, while the right panels provide a detailed analysis of the most affected areas, largely within the highest 40% of observation sensitivity as indicated by the green contour lines. The posterior fluxes are shown in Figures 2a and 2b, the flux differences between the posterior and prior in 2c and 2d, their ratio can be found in 2e and 2f, and the diagonal elements of the averaging kernel matrix in 2g and 2h. The averaging kernel sensitivity indicates where the inversion effectively updates the prior emissions based on observational constraints in the prior grid resolution. Error statistics on our inversion indicate that it provides eight independent pieces of information for the whole domain (measured by degrees of freedom for signal, DOFS).

Fluxes are reported in units of g m^{-2} yr^{-1} for comparability with annual emission inventories, but are derived from a 2-month period and thus represent temporally limited conditions rather than full annual means. However, comparing inter-annual flux variability of WetCHARTs from a 22-year climatology (see Figure S12 in Supporting Information S1), December and January - the dry to wet transition season - nearly represent an annual average, as the strongest emissions from wetlands are estimated during the wet season and the lowest emissions during the dry season. Overall, the inversion increases the basin-wide flux estimate by approximately ~5%, from 62.23 ± 5.04 Tg yr^{-1} in the prior to 65.68 ± 4.95 Tg yr^{-1} in the posterior, while substantially enhancing the spatial heterogeneity of the inferred flux distribution. Uncertainties represent the 1σ standard deviation estimated using Monte Carlo simulations. A detailed view on prior and posterior uncertainties can be found in the Figure S7 in Supporting Information S1.

We first focus on Figures 2a and 2b. In general, posterior emissions reflect the spatial pattern of the prior emissions, which capture the regional-scale spatial distribution of methane emission fluxes over Brazil (Hancock et al., 2025; Zhu et al., 2025). However, more detail in spatial flux variability could be achieved after the inversion due to the higher spatial resolution provided by the footprint matrix.

Regions with low observational sensitivities, which occur mainly the northwestern and southern part of our domain, show little change in emissions after the inversion (Figures 2c and 2d). Nevertheless, a few exceptions can be found in the east of Peru - a large wetland area - as well as in the large river delta of Venezuela on the northern edge of our domain, with changes of up to 50 g CH_4 m^{-2} yr^{-1}.

Within the region most strongly constrained by observations, we qualitatively see the largest previous underestimates in methane fluxes close to large river streams (e.g., the Amazon River) and in the Amazon delta, with posterior fluxes of up to 227.51 g CH_4 m^{-2} yr^{-1}. For comparison, the prior emissions within the spatial domain had a maximum methane flux of 103.45 g CH_4 m^{-2} yr^{-1}. The largest change in the posterior emissions relative to the prior is 152 g CH_4 m^{-2} yr^{-1}, which occurs southwest of the city of Manaus, Brazil, where large areas of seasonally flooded forests persist (3.7°S, 61.3°W). In general, the prior emissions inventory underestimated methane emissions across riverine systems.

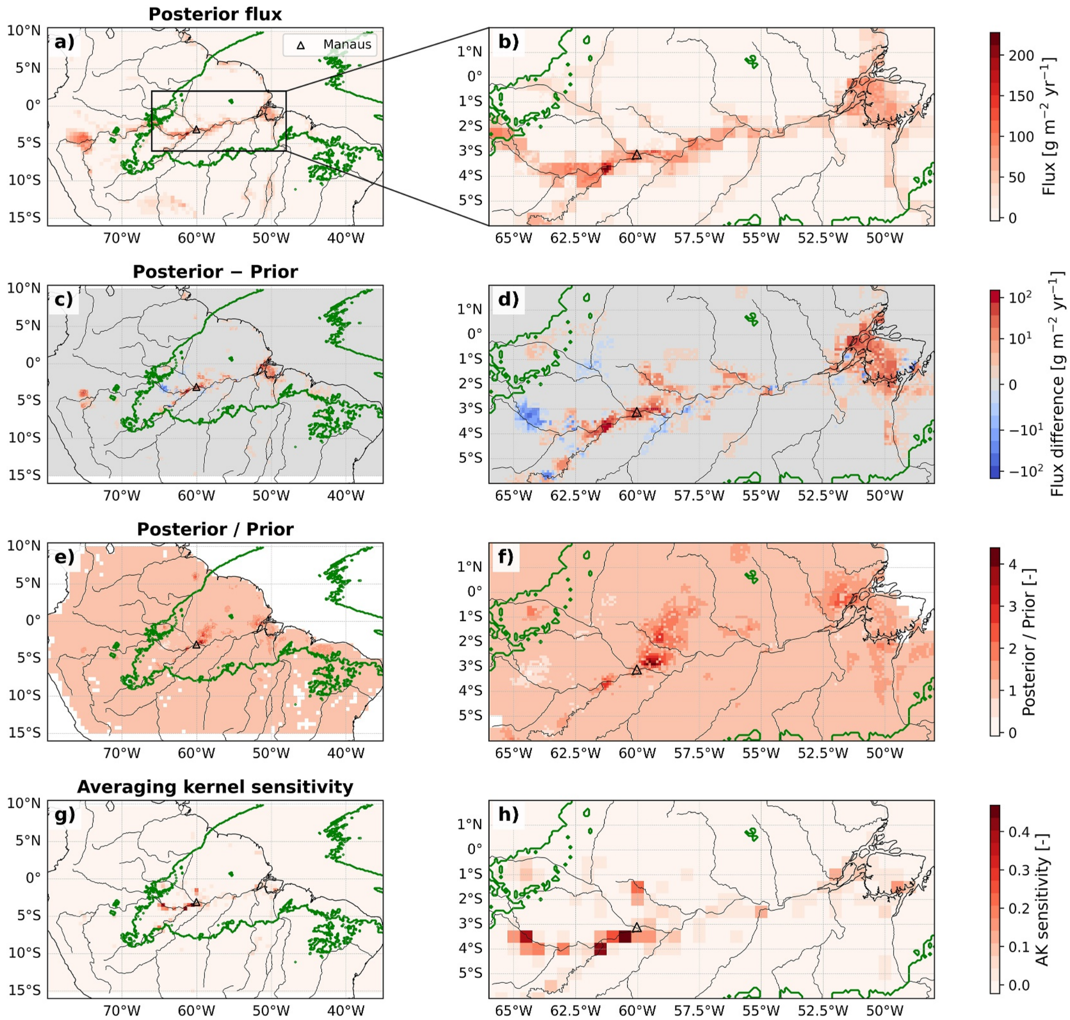

Figure 2. Posterior methane emissions over Amazonian basin. The left panels show posterior methane fluxes over the full Amazonian domain, with a close-up (black rectangle in panel (a)) shown on the right, both at 0.1° × 0.1° resolution. The posterior fluxes represent our optimized emission estimates obtained from the inversion, which uses WetCHARTs bottom-up fluxes as priors and is constrained by airborne methane observations (a, b). The difference between the posterior and the prior (c, d), and the ratio between the posterior and the prior (e, f), indicate the strongest change in emissions after the inversion in the Amazon delta and along river systems. The averaging kernel (AK) sensitivities represent the ability of the observations to quantify emissions independently from the prior estimates on the prior grid resolution (0.5° × 0.5°, (g, h). The green contour lines surround the area of the 40% strongest observational influence. The triangle marks the location of the city Manaus.

However, our inversion shows some regions where the WetCHARTs prior emissions are up to 50 g CH_4 m^{-2} yr^{-1} higher than the posterior, as indicated by blue colors in Figures 2c and 2d. In these regions, the bottom-up estimates seem to overestimate methane emissions, which may be due to higher surface complexity and vegetation properties, or under-constrained climate-induced feedback mechanisms such as localized drying of riverbeds resulting in more methane oxidation within soils (Stanley et al., 2016). WetCHARTs uses empirical, biogeochemical modeling with remotely sensed inundation, model-driven relative humidity fluxes, and a temperature sensitivity factor to estimate methane fluxes (Bloom et al., 2017; Zhu et al., 2025). Although WetCHARTs still captures small spatial details (see Figure S7 in Supporting Information S1), our inversion finds even stronger spatial heterogeneity, especially close to large river systems, mostly due to the inversion's higher resolution. However, WetCHARTs does not explicitly represent several processes that may contribute to the spatial heterogeneity of wetland-river methane emissions, including vegetation composition, macrophyte presence, hydrological state, flow velocity, and water depth.

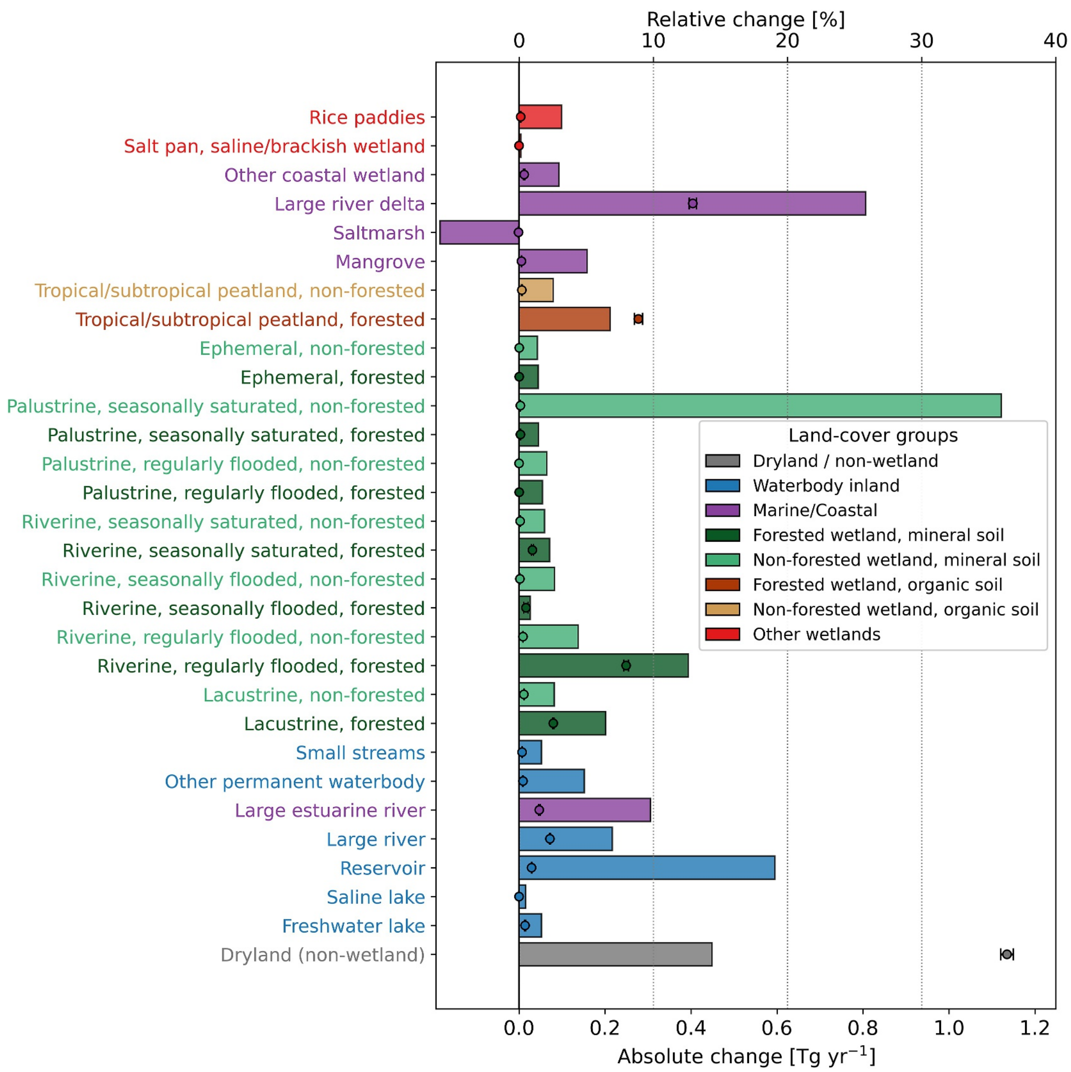

Figure 3. Land-cover–specific changes in methane emissions after inversion within the area of 40% highest observational sensitivity. Horizontal bars (top x-axis) show the prior-weighted relative change (%), where grid-cell contributions are weighted by their prior absolute flux within each land-cover classification by GLWD (same as used for spatial correlations of prior covariance matrix). Dots indicate the corresponding absolute change in class-integrated emissions ($\mathbf{\Delta F} = \hat{\mathbf{F}} - \mathbf{F}_p$; Tg yr^{-1}), with black error bars representing the 1σ uncertainty of total fluxes derived from 100 Monte Carlo realizations of the spatially correlated flux perturbations consistent with the inversion error covariance. Bar and dot colors indicate land-cover groupings (e.g., waterbody inland or marine/coastal, forested/non-forested, organic/mineral soils), adapted from Lehner et al. (2025b). A similar figure for the full domain can be found in Figure S11 of Supporting Information S1.

Comparing the ratio of posterior and prior fluxes (Figures 2e and 2f), we find that methane emissions are underestimated by the prior by up to a factor of four, mostly north of Manaus and in the Amazon River Delta. The region southwest of Manaus is most efficiently updated by the inversion, with AK sensitivities up to 0.48 (48% constrained by observations), which coincides with the area of highest fluxes in the posterior.

To identify which surface types drive the regional emission adjustment, we decompose the inversion-derived flux changes by land-cover class and quantify both their absolute and relative contributions. Figure 3 shows class-integrated absolute changes in methane emissions ($\mathbf{\Delta F} = \hat{\mathbf{F}} - \mathbf{F}_p$; Tg yr^{-1}) with 1$\sigma$ Monte Carlo uncertainties, together with the prior-weighted relative changes (%) for all land-cover types within the well-constrained area. Surface classifications are from GLWD (500 m at the equator) and re-gridded to our resolution via nearest-neighbor interpolation, assigning each cell the dominant land-cover class (see Figure S5 in

Supporting Information S1). We subdivide the land-cover types into colored main groups, according to Lehner et al. (2025b).

The strongest absolute change in wetland classifications can be found in coastal wetland regions, for example, large river deltas, mangroves, and large estuarine rivers. Notably, the spatially-averaged percentage corrections applied to the prior emissions were high for large river deltas (26%) and major estuarine rivers (10%), with post-inversion changes in total emissions of $+0.40 \pm 0.009$ Tg yr^{-1} and $+0.05 \pm 0.002$ Tg yr^{-1}, respectively. Methanogens decompose organic matter in waterlogged, anaerobic soils, producing methane via methanogenesis from substrates such as acetate and hydrogen. Conversely, methanotrophic bacteria oxidize methane to CO_2 or CH_3OH under oxic conditions (Murguia-Flores et al., 2018). Tropical soils exhibit intense microbial activity, often isolated from oxygen by extensive water bodies. River transport and deposition of organic matter can further distribute carbon substrates downstream. Methanogenesis in river sediments is strongly temperature-dependent and intensifies with warming (Yvon-Durocher et al., 2014). Rising temperatures enhance microbial metabolism and anaerobic carbon mineralization, increasing methane production. The growing frequency and intensity of river heatwaves, particularly in the Amazon and Congo Basin (Chen et al., 2026), elevate sediment temperatures and may reduce oxygen availability, potentially shifting rivers toward sustained methane production with distinct temporal emission regimes.

Furthermore, we observe strong relative changes and moderate absolute changes in methane fluxes in inland waterbodies, for example, reservoirs, large rivers, and permanent waterbodies. In particular, large rivers contribute $+0.07 \pm 0.001$ Tg yr^{-1} to the change in the regional budget, and reservoirs show a strong relative change of up to 19% in methane emissions, even though their absolute contribution is minor ($+0.029 \pm 0.0004$ Tg yr^{-1}). While there are limited studies about methane emissions from reservoirs (Delwiche et al., 2022; Michael Keller, 1994), there are growing concerns about the impact of the increasing number of hydropower stations in the Amazon (Caldas et al., 2023; Flecker et al., 2022). Early studies found that newly-built reservoirs in tropical regions (Gatun Lake, Panama) emit large amounts of methane via ebullition, with fluxes of 3.65 – 73 g CH_4 m^{-2} yr^{-1} at deeper sites (>7 m) and 730 g CH_4 m^{-2} yr^{-1} at shallow sites (<2 m) (Michael Keller, 1994). Furthermore, substantial inundation of forested regions for hydropower energy recovery often results in dead trees in the lakes due to deficient forest clearing (Caldas et al., 2023). Consequently, the presence of dead tree-stumps in the inundated area could function as a carbon conduit, facilitating the transfer of methane from the underlying soil to the atmosphere.

Across forested and non-forested zones with both organic and mineral soils (e.g., riverine, regularly flooded, forested; palustrine, non-forested, seasonally-flooded; Lacustrine, forested; tropical/subtropical peatland, forested), methane emissions show moderate increases after inversion. Of these biomes, regularly-flooded riverine and tropical peatland contribute most to the regional budget adjustment, with absolute and relative changes of $+0.25 \pm 0.005$ Tg yr^{-1} (13%), and $+0.28 \pm 0.009$ Tg yr^{-1} (7%), respectively. Non-forested, seasonally-flooded palustrine areas show a strong relative change (36%) because of the small prior emission flux (not shown); however, their absolute contribution is nearly zero ($+0.003 \pm 0.00005$ Tg yr^{-1}).

We expect pronounced seasonal variability in wetland emissions according to WetCHARTs (Figure S12 in Supporting Information S1), supported by bi-weekly annual observations (Basso et al., 2021), with peaking wetland emissions during the wet season (March–April) and smallest wetland emissions during the dry season (July–October), along with increasing influence of biomass burning emissions. Reported fluxes are annualized from the December–January observations and should be interpreted under the assumption that the dry-to-wet transition season is broadly representative of the annual mean, with wetland emissions expected to reflect intermediate conditions between the dry- and wet-season extremes. Comparing annual WetCHARTs means to those annualized December–January fluxes reveals a north-south contrast: December–January fluxes are ~30 g CH_4 m^{-2} yr^{-1} higher than the annual average south of the Amazon River and ~30 g CH_4 m^{-2} yr^{-1} lower in the northern Amazon (Figure S8 in Supporting Information S1). Tropical ecosystems are changing rapidly through warmer temperatures and altered precipitation patterns, resulting in strong seasonal and regional differences in water levels, temperatures, and methane emissions. Anthropogenic land-use in the Amazon has increased dramatically over the last decades, increasing not only methane emissions from livestock, but also impacting forested peatlands, which contain large amounts of carbon (Girkin et al., 2022).

Additionally, we find the greatest absolute change in methane total emissions in dryland cells (+1.14 ± 0.015 Tg yr^{-1} or +14%). This could include methane emissions from sources other than wetlands, such as livestock, landfills, wastewater, or other anthropogenic sources. Although current emission inventories suggest a minor contribution of those sources on the regional-scale in central Amazonia (see Figures S13–S15 in Supporting Information S1). However, those enhanced posterior emissions may also arise, to some extent, from spatial aggregation effects, namely mixing dryland with wetland fractions which would bias grid-scale fluxes high. Moreover, methane emissions coming from regions GLWD has not classified as wetlands might be experiencing inundation (Balasus et al., 2026). Possible surface property changes may also contribute to that enhancement, as those are highly affected by climate change (Franco et al., 2025) and are not considered in the WetCHARTs inventory.

4. Conclusions and Outlook

The tropics are important methane source regions. In particular, the Amazon rain forest is a highly complex region with a variable and sensitive ecosystem, particularly in the context of climate change. Better quantifying its changing contribution to greenhouse gas fluxes is key in global total emissions and carbon cycling. In this study, we used airborne observations of methane from the dry-to-wet transition season (December 2022–January 2023) above the Amazon rain forest to evaluate current bottom-up methane emission estimates using a footprint analysis and a Bayesian inversion. We focused on wetland emissions, which are the strongest methane emitters in the tropics. While WetCHARTs bottom-up emissions provided a good estimate of methane fluxes for most of the Amazon Basin after our inversion, some regional fluxes were estimated to be up to four times larger than WetCHARTs. We found the largest changes between the prior and posterior in large river deltas, reservoirs, and river systems in the Amazon. Spatial variability of methane fluxes highly depend on small-scale surface properties (e.g., microbial activity, saturation), where even small rivers and lakes can emit large amounts of methane.

Our inversion results suggest large underestimations of methane fluxes across wetland-river continuum, particularly at the estuaries of the Amazon, where large volumes of freshwater enters the Atlantic. These results are consistent with other recent modeling studies, suggesting a strong regional-scale wetland source of the Amazon, transported across the domain (Benavente et al., 2026). Beyond revealing previously unobserved fluxes, our results highlight the urgent need to better characterize the processes controlling methanogenesis across the tropical aquatic continuum. The important role of soil microbes as sources and sinks of methane is not yet well understood, especially in a changing climate. Temperature sensitivity and deposition of eroded soils containing large amounts of organic matter in coastal regions needs to be considered for carbon emissions, and not only for the Amazon. Similar biases could extend to other tropical river systems in Central Africa (Balasus et al., 2026), and Southeast Asia, where observational constraints remain sparse and process representation is uncertain. Anthropogenic activities are increasingly affecting tropical ecosystems, in land-use change and climate feedback mechanism, underscoring the need for more accurate attribution of top-down fluxes to the multiple, overlapping processes contributing to methane emissions (Pangala et al., 2017). Improved observational coverage and model representation of tropical large rivers, deltas, flooded forests, peatlands, and reservoirs, are therefore critical for reducing uncertainties, capturing small-scale variability, and solving temporal dynamics in the global methane budget.

Conflict of Interest

The authors declare no conflicts of interest relevant to this study.

Availability Statement

Observational data used in this study can be obtained on the HALO database platform by signing a data contract (DLR, 2023) or can be found, together with the model data used in this study on Zenodo via Ort et al. (2026). CAMS data (release: v23r1, source: TM5-MP 4D-Var) was downloaded via (Copernicus Atmosphere Monitoring Service, 2020) [last access: 7 March 2025]. WetCHARTs ensemble simulations can be accessed via Bloom et al. (2024) and are explained in detail in Bloom et al. (2017). The GLWD data set can be found via Lehner et al. (2025a), and is explained in Lehner et al. (2025b) and Lehner and Döll (2004).

Acknowledgments
We acknowledge all participants from the CAFE Brazil campaign and those who helped develop the models. In particular, we thank all local Brazilian researchers, specifically Paulo Artaxo and Luiz A. T. Machado, for their essential logistical and organizational work making the CAFE Brazil campaign possible in the first place. We further thank Uwe Parchatka and Lenard Röder for their technical and analytical support with the methane measurements. ND, JYY, and AJT were supported by Schmidt Sciences through the VESRI program and the $FETCH_4$ project. Part of this research was carried out at the Jet Propulsion Laboratory, California Institute of Technology, under a contract with the National Aeronautics and Space Administration. Open Access funding enabled and organized by Projekt DEAL.

References

Andreae, M. O., Artaxo, P., Beck, V., Bela, M., Freitas, S., Gerbig, C., et al. (2012). Carbon monoxide and related trace gases and aerosols over the Amazon Basin during the wet and dry seasons. *Atmospheric Chemistry and Physics*, *12*(13), 6041–6065. https://doi.org/10.5194/acp-12-6041-2012

Asner, G. P. (2001). Cloud cover in Landsat observations of the Brazilian Amazon. *International Journal of Remote Sensing*, *22*(18), 3855–3862. https://doi.org/10.1080/01431160010006926

Balasus, N., Jacob, D. J., Bloom, A. A., East, J. D., Estrada, L. A., Hancock, S. E., et al. (2026). 2019–2024 trends in African livestock and wetland emissions as contributors to the global methane rise. *EGUsphere*, 1–30. https://doi.org/10.5194/egusphere-2025-6251

Basso, L. S., Marani, L., Gatti, L. V., Miller, J. B., Gloor, M., Melack, J., et al. (2021). Amazon methane budget derived from multi-year airborne observations highlights regional variations in emissions. *Communications Earth & Environment*, *2*(1), 246. https://doi.org/10.1038/s43247-021-00314-4

Beck, V., Chen, H., Gerbig, C., Bergamaschi, P., Bruhwiler, L., Houweling, S., et al. (2012). Methane airborne measurements and comparison to global models during BARCA. *Journal of Geophysical Research*, *117*(D15). https://doi.org/10.1029/2011JD017345

Benavente, R., Botía, S., Rizzo, V., Vara-Vela, A., Artaxo, P., van Asperen, H., et al. (2026). Assessment of WRF-GHG model simulations during the CAFE-Brazil Campaign in Amazonia. *EGUsphere*, 1–32. https://doi.org/10.5194/egusphere-2026-979

Bey, I., Jacob, D. J., Yantosca, R. M., Logan, J. A., Field, B. D., Fiore, A. M., et al. (2001). Global modeling of tropospheric chemistry with assimilated meteorology: Model description and evaluation. *Journal of Geophysical Research*, *106*(D19), 23073–23095. https://doi.org/10.1029/2001JD000807

Bloom, A. A., Bowman, K. W., Lee, M., Turner, A. J., Schroeder, R., Worden, J. R., et al. (2024). CMS: Global 0.5-deg wetland methane emissions and uncertainty (WetCHARTs v1.3.3) [Dataset]. *ORNL Distributed Active Archive Center*. https://doi.org/10.3334/ORNLDAAC/2346

Bloom, A. A., Bowman, K. W., Lee, M., Turner, A. J., Schroeder, R., Worden, J. R., et al. (2017). A global wetland methane emissions and uncertainty dataset for atmospheric chemical transport models (WetCHARTs version 1.0). *Geoscientific Model Development*, *10*(6), 2141–2156. https://doi.org/10.5194/gmd-10-2141-2017

Caldas, B., Thieme, M. L., Shahbol, N., Coelho, M. E., Grill, G., Van Damme, P. A., et al. (2023). Identifying the current and future status of freshwater connectivity corridors in the Amazon Basin. *Conservation Science and Practice*, *5*(1), e12853. https://doi.org/10.1111/csp2.12853

Chen, S., Yuan, K., Li, F., Zhu, Q., & Zhuang, Q. (2025). Hysteretic temperature sensitivity in wetland CH4 emission modeling. *Agricultural and Forest Meteorology*, *372*, 110704. https://doi.org/10.1016/j.agrformet.2025.110704

Chen, Y., Su, Z., Woolway, R. I., Wanders, N., Wu, S., Huang, Z., & Luo, M. (2026). Persistent river heatwaves are emerging worldwide under climate change. *Nature Communications*, *17*(1), 94. https://doi.org/10.1038/s41467-025-66868-5

Copernicus Atmosphere Monitoring Service. (2020). CAMS global inversion-optimised greenhouse gas fluxes and concentrations [Dataset]. *Copernicus Atmosphere Monitoring Service (CAMS) Atmosphere Data Store*. https://doi.org/10.24381/ed2851d2

Curtius, J., Heinritzi, M., Beck, L. J., Pöhlker, M. L., Tripathi, N., Krumm, B. E., et al. (2024). Isoprene nitrates drive new particle formation in Amazon's upper troposphere. *Nature*, *636*(8041), 124–130. https://doi.org/10.1038/s41586-024-08192-4

Cusworth, D. H., Thorpe, A. K., Ayasse, A. K., Stepp, D., Heckler, J., Asner, G. P., et al. (2022). Strong methane point sources contribute a disproportionate fraction of total emissions across multiple basins in the United States. *Proceedings of the National Academy of Sciences*, *119*(38), e2202338119. https://doi.org/10.1073/pnas.2202338119

Dadheech, N., He, T.-L., & Turner, A. J. (2025). High-resolution greenhouse gas flux inversions using a machine learning surrogate model for atmospheric transport. *Atmospheric Chemistry and Physics*, *25*(10), 5159–5174. https://doi.org/10.5194/acp-25-5159-2025

Delwiche, K. B., Harrison, J. A., Maasakkers, J. D., Sulprizio, M. P., Worden, J., Jacob, D. J., & Sunderland, E. M. (2022). Estimating drivers and pathways for Hydroelectric Reservoir methane emissions using a new mechanistic model. *Journal of Geophysical Research: Biogeosciences*, *127*(8), e2022JG006908. https://doi.org/10.1029/2022JG006908

Delwiche, K. B., Knox, S. H., Malhotra, A., Fluet-Chouinard, E., McNicol, G., Feron, S., et al. (2021). FLUXNET-CH4: A global, multi-ecosystem dataset and analysis of methane seasonality from freshwater wetlands. *Earth System Science Data*, *13*(7), 3607–3689. https://doi.org/10.5194/essd-13-3607-2021

Dhakal, S., Minx, J. C., Toth, F. L., Abdel-Aziz, A., Figueroa Meza, M. J., Hubacek, K., et al. (Eds.), Climate change 2022: Mitigation of climate change. Cambridge University Press. https://doi.org/10.1017/9781009157926.004

DLR. (2023). HALO data-base, CAFE Brazil [Dataset]. *German Aerospace Center (DLR)*. Retrieved from https://halo-db.pa.op.dlr.de/mission/135

Dutaur, L., & Verchot, L. V. (2007). A global inventory of the soil ch4 sink. *Global Biogeochemical Cycles*, *21*(4). https://doi.org/10.1029/2006GB002734

Flecker, A. S., Shi, Q., Almeida, R. M., Angarita, H., Gomes-Selman, J. M., García-Villacorta, R., et al. (2022). Reducing adverse impacts of Amazon hydropower expansion. *Science*, *375*(6582), 753–760. https://doi.org/10.1126/science.abj4017

France, J. L., Lunt, M. F., Andrade, M., Moreno, I., Ganesan, A. L., Lachlan-Cope, T., et al. (2022). Very large fluxes of methane measured above Bolivian seasonal wetlands. *Proceedings of the National Academy of Sciences*, *119*(32), e2206345119. https://doi.org/10.1073/pnas.2206345119

Franco, M. A., Rizzo, L. V., Teixeira, M. J., Artaxo, P., Azevedo, T., Lelieveld, J., et al. (2025). How climate change and deforestation interact in the transformation of the Amazon rainforest. *Nature Communications*, *16*(1), 7944. https://doi.org/10.1038/s41467-025-63156-0

Frankenberg, C., Thorpe, A. K., Thompson, D. R., Hulley, G., Kort, E. A., Vance, N., et al. (2016). Airborne methane remote measurements reveal heavy-tail flux distribution in four corners region. *Proceedings of the National Academy of Sciences*, *113*(35), 9734–9739. https://doi.org/10.1073/pnas.1605617113

Girkin, N. T., Cooper, H. V., Ledger, M. J., O'Reilly, P., Thornton, S. A., Åkesson, C. M., et al. (2022). Tropical peatlands in the Anthropocene: The present and the future. *Anthropocene*, *40*, 100354. https://doi.org/10.1016/j.ancene.2022.100354

Hancock, S. E., Jacob, D. J., Chen, Z., Nesser, H., Davitt, A., Varon, D. J., et al. (2025). Satellite quantification of methane emissions from South American countries: A high-resolution inversion of TROPOMI and GOSAT observations. *Atmospheric Chemistry and Physics*, *25*(2), 797–817. https://doi.org/10.5194/acp-25-797-2025

He, Z., Gao, L., Liang, M., & Zeng, Z.-C. (2024). A survey of methane point source emissions from coal mines in Shanxi province of China using AHSI on board Gaofen-5B. *Atmospheric Measurement Techniques*, *17*(9), 2937–2956. https://doi.org/10.5194/amt-17-2937-2024

Henze, D. K., Hakami, A., & Seinfeld, J. H. (2007). Development of the adjoint of GEOS-Chem. *Atmospheric Chemistry and Physics*, *7*(9), 2413–2433. https://doi.org/10.5194/acp-7-2413-2007

Hutchinson, M. (1989). A stochastic estimator of the trace of the influence matrix for laplacian smoothing splines. *Communications in Statistics - Simulation and Computation*, *18*(3), 1059–1076. https://doi.org/10.1080/03610918908812806

Jackson, R. B., Saunois, M., Bousquet, P., Canadell, J. G., Poulter, B., Stavert, A. R., et al. (2020). Increasing anthropogenic methane emissions arise equally from agricultural and fossil fuel sources. *Environmental Research Letters*, *15*(7), 071002. https://doi.org/10.1088/1748-9326/ab9ed2

Jacob, D. J., Varon, D. J., Cusworth, D. H., Dennison, P. E., Frankenberg, C., Gautam, R., et al. (2022). Quantifying methane emissions from the global scale down to point sources using satellite observations of atmospheric methane. *Atmospheric Chemistry and Physics*, *22*(14), 9617–9646. https://doi.org/10.5194/acp-22-9617-2022

Knox, S. H., Jackson, R. B., Poulter, B., McNicol, G., Fluet-Chouinard, E., Zhang, Z., et al. (2019). FLUXNET-CH4 synthesis activity: Objectives, observations, and future directions. *Bulletin of the American Meteorological Society*, *100*(12), 2607–2632. https://doi.org/10.1175/BAMS-D-18-0268.1

Konopka, P., Ploeger, F., D'Amato, F., Campos, T., von Hobe, M., Honomichl, S. B., et al. (2025). Isentropic mixing vs. convection in CLaMS-3.0/MESSy: Evaluation using satellite climatologies and in situ carbon monoxide observations. *Atmospheric Chemistry and Physics*, *25*(23), 17973–17996. https://doi.org/10.5194/acp-25-17973-2025

Lan, X., Thoning, K., & Dlugokencky, E. (2025). Trends in globally-averaged CH4, N2O, and SF6 determined from NOAA Global Monitoring Laboratory measurements. Version 2025-03. https://doi.org/10.15138/P8XG-AA10

Lehner, B., Anand, M., Fluet-Chouinard, E., Tan, F., Aires, F., Allen, G. H., et al. (2025a). Global Lakes and Wetlands Database (GLWD) version 2.0 [Dataset]. https://doi.org/10.6084/m9.figshare.28519994.v1

Lehner, B., Anand, M., Fluet-Chouinard, E., Tan, F., Aires, F., Allen, G. H., et al. (2025b). Mapping the world's inland surface waters: An upgrade to the Global Lakes and Wetlands Database (GLWD v2). *Earth System Science Data*, *17*(6), 2277–2329. https://doi.org/10.5194/essd-17-2277-2025

Lehner, B., & Döll, P. (2004). Development and validation of a global database of lakes, reservoirs and wetlands. *Journal of Hydrology*, *296*(1), 1–22. https://doi.org/10.1016/j.jhydrol.2004.03.028

Lin, J. C., Gerbig, C., Wofsy, S. C., Andrews, A. E., Daube, B. C., Davis, K. J., & Grainger, C. A. (2003). A near-field tool for simulating the upstream influence of atmospheric observations: The Stochastic Time-Inverted Lagrangian Transport (STILT) model. *Journal of Geophysical Research*, *108*(D16). https://doi.org/10.1029/2002JD003161

Lu, X., Jacob, D. J., Zhang, Y., Maasakkers, J. D., Sulprizio, M. P., Shen, L., et al. (2021). Global methane budget and trend, 2010–2017: Complementarity of inverse analyses using in situ (GLOBALVIEWplus CH4 ObsPack) and satellite (GOSAT) observations. *Atmospheric Chemistry and Physics*, *21*(6), 4637–4657. https://doi.org/10.5194/acp-21-4637-2021

Maasakkers, J. D., Jacob, D. J., Sulprizio, M. P., Scarpelli, T. R., Nesser, H., Sheng, J.-X., et al. (2019). Global distribution of methane emissions, emission trends, and OH concentrations and trends inferred from an inversion of GOSAT satellite data for 2010–2015. *Atmospheric Chemistry and Physics*, *19*(11), 7859–7881. https://doi.org/10.5194/acp-19-7859-2019

Malley, C. S., Borgford-Parnell, N., Haeussling, S., Howard, I. C., Lefèvre, E. N., & Kuylenstierna, J. C. I. (2023). A roadmap to achieve the global methane pledge. *Environmental Research: Climate*, *2*(1), 011003. https://doi.org/10.1088/2752-5295/acb4b4

McKenna, D. S., Grooß, J.-U., Günther, G., Konopka, P., Müller, R., Carver, G., & Sasano, Y. (2002). A new Chemical Lagrangian Model of the Stratosphere (CLaMS) 2. Formulation of chemistry scheme and initialization. *Journal of Geophysical Research*, *107*(D15). https://doi.org/10.1029/2000JD000113

McKenna, D. S., Konopka, P., Grooß, J.-U., Günther, G., Müller, R., Spang, R., et al. (2002). A new Chemical Lagrangian Model of the Stratosphere (CLaMS) 1. Formulation of advection and mixing. *Journal of Geophysical Research*, *107*(D16). https://doi.org/10.1029/2000JD000114

Michael Keller, R. F. S. (1994). Methane emission by bubbling from Gatun Lake, Panama. *Journal of Geophysical Research*, *99*(D4), 8307–8319. https://doi.org/10.1029/92JD02170

Murguia-Flores, F., Arndt, S., Ganesan, A. L., Murray-Tortarolo, G., & Hornibrook, E. R. C. (2018). Soil Methanotrophy Model (MeMo v1.0): A process-based model to quantify global uptake of atmospheric methane by soil. *Geoscientific Model Development*, *11*(6), 2009–2032. https://doi.org/10.5194/gmd-11-2009-2018

Nisbet, E. G., Manning, M. R., Dlugokencky, E. J., Fisher, R. E., Lowry, D., Michel, S. E., et al. (2019). Very strong atmospheric methane growth in the 4 years 2014–2017: Implications for the paris agreement. *Global Biogeochemical Cycles*, *33*(3), 318–342. https://doi.org/10.1029/2018GB006009

Niwa, Y., Tohjima, Y., Terao, Y., Saeki, T., Ito, A., Umezawa, T., et al. (2025). Multi-observational estimation of regional and sectoral emission contributions to the persistent high growth rate of atmospheric CH4 for 2020–2022. *Atmospheric Chemistry and Physics*, *25*(13), 6757–6785. https://doi.org/10.5194/acp-25-6757-2025

Nussbaumer, C. M., Kohl, M., Pozzer, A., Tadic, I., Rohloff, R., Marno, D., et al. (2024). Ozone formation sensitivity to precursors and lightning in the tropical troposphere based on airborne observations. *Journal of Geophysical Research: Atmospheres*, *129*(14), e2024JD041168. https://doi.org/10.1029/2024JD041168

Ort, L., Dadheech, N., Yoon, J., Turner, A., Bloom, A. A., Lachnitt, H.-C., et al. (2026). Supporting data for: Airborne observations reveal underestimated riverine methane emissions across the Amazon [Dataset]. *Zenodo*. https://doi.org/10.5281/zenodo.18504592

Ort, L., Röder, L. L., Parchatka, U., Königstedt, R., Crowley, D., Kunz, F., et al. (2024). In-flight characterization of a compact airborne quantum cascade laser absorption spectrometer. *Atmospheric Measurement Techniques*, *17*(11), 3553–3565. https://doi.org/10.5194/amt-17-3553-2024

Pangala, S. R., Enrich-Prast, A., Basso, L. S., Peixoto, R. B., Bastviken, D., Hornibrook, E. R. C., et al. (2017). Large emissions from floodplain trees close the amazon methane budget. *Nature*, *552*(7684), 230–234. https://doi.org/10.1038/nature24639

Pérez-Domínguez, I., Del Prado, A., Mittenzwei, K., Hristov, J., Frank, S., Tabeau, A., et al. (2021). Short-and long-term warming effects of methane may affect the cost-effectiveness of mitigation policies and benefits of low-meat diets. *Nature Food*, *2*(12), 970–980. https://doi.org/10.1038/s43016-021-00385-8

Prather, M. J., Holmes, C. D., & Hsu, J. (2012). Reactive greenhouse gas scenarios: Systematic exploration of uncertainties and the role of atmospheric chemistry. *Geophysical Research Letters*, *39*(9). https://doi.org/10.1029/2012GL051440

Predybaylo, E., Lelieveld, J., Pozzer, A., Gromov, S., Zimmermann, P., Osipov, S., et al. (2025). Surface temperature and ozone responses to the 2030 Global Methane Pledge. *Climatic Change*, *178*(4), 78. https://doi.org/10.1007/s10584-025-03908-5

Prein, A. F., Langhans, W., Fosser, G., Ferrone, A., Ban, N., Goergen, K., et al. (2015). A review on regional convection-permitting climate modeling: Demonstrations, prospects, and challenges. *Reviews of Geophysics*, *53*(2), 323–361. https://doi.org/10.1002/2014RG000475

Röder, L. L., Ort, L., Lelieveld, J., & Fischer, H. (2024). Quantitative analysis of temporal stability and instrument performance during field experiments of an airborne QCLAS via allan–werle–plots. *Applied Physics B*, *130*(7), 118. https://doi.org/10.1007/s00340-024-08254-5

Rodgers, C. D. (1990). Characterization and error analysis of profiles retrieved from remote sounding measurements. *Journal of Geophysical Research*, *95*(D5), 5587–5595. https://doi.org/10.1029/JD095iD05p05587

Rodgers, C. D. (2000). Inverse methods for atmospheric sounding: Theory and practice. *World scientific*.

Saunois, M., Martinez, A., Poulter, B., Zhang, Z., Raymond, P., Regnier, P., et al. (2024). Global methane budget 2000–2020. *Earth System Science Data Discussions*, *2024*, 1–147. https://doi.org/10.5194/essd-2024-115

Saunois, M., Martinez, A., Poulter, B., Zhang, Z., Raymond, P. A., Regnier, P., et al. (2025). Global Methane Budget 2000–2020. *Earth System Science Data*, *17*(5), 1873–1958. https://doi.org/10.5194/essd-17-1873-2025

Saunois, M., Stavert, A. R., Poulter, B., Bousquet, P., Canadell, J. G., Jackson, R. B., et al. (2020). The Global Methane Budget 2000–2017. *Earth System Science Data*, *12*(3), 1561–1623. https://doi.org/10.5194/essd-12-1561-2020

Scheuer, E. M., & Stoller, D. S. (1962). On the generation of normal random vectors. *Technometrics*, *4*(2), 278–281. https://doi.org/10.1080/00401706.1962.10490011

Shindell, D., Kuylenstierna, J. C. I., Vignati, E., van Dingenen, R., Amann, M., Klimont, Z., et al. (2012). Simultaneously mitigating near-term climate change and improving human health and food security. *Science*, *335*(6065), 183–189. https://doi.org/10.1126/science.1210026

Silva Junior, C. H. L., Pessôa, A. C. M., Carvalho, N. S., Reis, J. B. C., Anderson, L. O., & Aragão, L. E. O. C. (2021). The brazilian amazon deforestation rate in 2020 is the greatest of the decade. *Nature Ecology & Evolution*, *5*(2), 144–145. https://doi.org/10.1038/s41559-020-01368-x

Stanley, E. H., Casson, N. J., Christel, S. T., Crawford, J. T., Loken, L. C., & Oliver, S. K. (2016). The ecology of methane in streams and rivers: Patterns, controls, and global significance. *Ecological Monographs*, *86*(2), 146–171. https://doi.org/10.1890/15-1027

Tarantola, A. (2005). *Inverse problem theory and methods for model parameter estimation*. Society for Industrial and Applied Mathematics (SIAM). (Completely rewritten edition of the 1987 volume).

Turner, A. J., Frankenberg, C., & Kort, E. A. (2019). Interpreting contemporary trends in atmospheric methane. *Proceedings of the National Academy of Sciences*, *116*(8), 2805–2813. https://doi.org/10.1073/pnas.1814297116

Turner, A. J., Jacob, D. J., Benmergui, J., Brandman, J., White, L., & Randles, C. A. (2018). Assessing the capability of different satellite observing configurations to resolve the distribution of methane emissions at kilometer scales. *Atmospheric Chemistry and Physics*, *18*(11), 8265–8278. https://doi.org/10.5194/acp-18-8265-2018

Turner, A. J., Kim, J., Fitzmaurice, H., Newman, C., Worthington, K., Chan, K., et al. (2020). Observed impacts of COVID-19 on urban CO2 emissions. *Geophysical Research Letters*, *47*(22), e2020GL090037. https://doi.org/10.1029/2020GL090037

Uluocak, I. (2025). Hybrid deep learning models for predicting atmospheric methane concentrations: A comparative analysis through 2050. *Science China Earth Sciences*, *68*(7), 1–11. https://doi.org/10.1007/s11430-024-1569-9

Yvon-Durocher, G., Allen, A. P., Bastviken, D., Conrad, R., Gudasz, C., St-Pierre, A., et al. (2014). Methane fluxes show consistent temperature dependence across microbial to ecosystem scales. *Nature*, *507*(7493), 488–491. https://doi.org/10.1038/nature13164

Zhang, Z., Zimmermann, N. E., Stenke, A., Li, X., Hodson, E. L., Zhu, G., et al. (2017). Emerging role of wetland methane emissions in driving 21st century climate change. *Proceedings of the National Academy of Sciences*, *114*(36), 9647–9652. https://doi.org/10.1073/pnas.1618765114

Zhu, Q., Jacob, D. J., Yuan, K., Li, F., Runkle, B. R. K., Chen, M., et al. (2025). Advancements and opportunities to improve bottom–up estimates of global wetland methane emissions. *Environmental Research Letters*, *20*(2), 023001. https://doi.org/10.1088/1748-9326/adad02

References From the Supporting Information

Andreae, M. O., Acevedo, O. C., Ara`ujo, A., Artaxo, P., Barbosa, C. G. G., Barbosa, H. M. J., et al. (2015). The Amazon Tall Tower Observatory (ATTO): Overview of pilot measurements on ecosystem ecology, meteorology, trace gases, and aerosols. *Atmospheric Chemistry and Physics*, *15*(18), 10723–10776. https://doi.org/10.5194/acp-15-10723-2015

Ba, Y. A., Wenger, C., Surleau, R., Boudon, V., Rotger, M., Daumont, L., et al. (2013). Mecasda and ecasda: Methane and ethene calculated spectroscopic databases for the virtual atomic and molecular data centre. *Journal of Quantitative Spectroscopy and Radiative Transfer*, *130*, 62–68. https://doi.org/10.1016/j.jqsrt.2013.05.001

Bergamaschi, P., Houweling, S., Segers, A., Krol, M., Frankenberg, C., Scheepmaker, R. A., et al. (2013). Atmospheric CH4 in the first decade of the 21st century: Inverse modeling analysis using SCIAMACHY satellite retrievals and NOAA surface measurements. *Journal of Geophysical Research: Atmospheres*, *118*(13), 7350–7369. https://doi.org/10.1002/jgrd.50480

Colligan, T., Poulter, B., & Quinn, C. (2024). LPJ-EOSIM L2 global simulated daily Wetland Methane flux V001 [Dataset]. *NASA Land Processes Distributed Active Archive Center*. https://doi.org/10.5067/comMUNITY/LPJ-EOSIM/LPJ_EOSIM_L2_DCH4E.001

DLR. (2025). HALO. German aerospace Center (DLR) [Software]. Retrieved from https://www.dlr.de/en/research-and-transfer/projects-and-missions/halo-high-altitude-and-long-range-research-aircraft

Fung, I., John, J., Lerner, J., Matthews, E., Prather, M., Steele, L. P., & Fraser, P. J. (1991). Three-dimensional model synthesis of the global methane cycle. *Journal of Geophysical Research*, *96*(D7), 13033–13065. https://doi.org/10.1029/91JD01247

Haracono, Y., Iwata, H., Sakabe, A., Ueyama, M., Takahashi, K., Nagano, H., et al. (2015). Effects of water vapor dilution on trace gas flux, and practical correction methods. *Journal of Agricultural Meteorology*, *71*(2), 65–76. https://doi.org/10.2480/agrmet.D-14-00003

Herriott, D. R., & Schulte, H. J. (1965). Folded optical delay lines. *Applied Optics*, *4*(8), 883–889. https://doi.org/10.1364/AO.4.000883

Hersbach, H., Bell, B., Berrisford, P., Hirahara, S., Horányi, A., Muñoz-Sabater, J., et al. (2020). The ERA5 global reanalysis. *Quarterly Journal of the Royal Meteorological Society*, *146*(730), 1999–2049. https://doi.org/10.1002/qj.3803

Kaufmann, S., Voigt, C., Heller, R., Jurkat-Witschas, T., Krämer, M., Rolf, C., et al. (2018). Intercomparison of midlatitude tropospheric and lower-stratospheric water vapor measurements and comparison to ECMWF humidity data. *Atmospheric Chemistry and Physics*, *18*(22), 16729–16745. https://doi.org/10.5194/acp-18-16729-2018

Kindel, B., Pilewskie, P., Schmidt, K., Thornberry, T., Rollins, A., & Bui, T. (2015). 03). Upper-troposphere and lower-stratosphere water vapor retrievals from the 1400 and 1900 nm water vapor bands. *Atmospheric Measurement Techniques*, *8*(3), 1147–1156. https://doi.org/10.5194/amt-8-1147-2015

Li, G., Gordon, I. E., Rothman, L. S., Tan, Y., Hu, S.-M., Kassi, S., et al. (2015). Rovibrational line lists for nine isotopologues of the CO molecule in the X1Σ+ ground electronic state. *The Astrophysical Journal Supplement Series*, *216*(1), 15. https://doi.org/10.1088/0067-0049/216/1/15

Messager, M. L., Lehner, B., Grill, G., Nedeva, I., & Schmitt, O. (2016). Estimating the volume and age of water stored in global lakes using a geo-statistical approach. *Nature Communications*, *7*(1), 13603. https://doi.org/10.1038/ncomms13603

Pommrich, R., Müller, R., Grooß, J.-U., Konopka, P., Ploeger, F., Vogel, B., et al. (2014). Tropical troposphere to stratosphere transport of carbon monoxide and long-lived trace species in the chemical lagrangian model of the stratosphere (clams). *Geoscientific Model Development*, *7*(6), 2895–2916. https://doi.org/10.5194/gmd-7-2895-2014

Tomsche, L., Pozzer, A., Ojha, N., Parchatka, U., Lelieveld, J., & Fischer, H. (2019). Upper tropospheric ch 4 and co affected by the south asian summer monsoon during the oxidation mechanism observations mission. *Atmospheric Chemistry and Physics*, *19*(3), 1915–1939. https://doi.org/10.5194/acp-19-1915-2019

Toth, R. (2004). Linelist of N2O parameters from 500 to 7500 cm−1.JPL online

Wienhold, F., Fischer, H., Hoor, P., Wagner, V., Königstedt, R., Harris, G., et al. (1998). Tristar-a tracer in-situ tdlas for atmospheric research. *Applied Physics B*, *67*(4), 411–417. https://doi.org/10.1007/s003400050524